Operando X-ray Diffraction Study of Mn−Ce Catalysts for CO Oxidation

Z. S. Vinokurov[a, b,]*, T. N. Afonasenko[c], D. D. Mishchenko[a, b], A. A. Saraev[a, b], E. E. Aydakov[a],
V. A. Rogov[a], and O. A. Bulavchenko[a]

[a] Boreskov Institute of Catalysis, Siberian Branch, Russian Academy of Sciences, Novosibirsk, 630090 Russia
[b] Synchrotron Radiation Facility SKIF, Boreskov Institute of Catalysis, Siberian Branch, Russian Academy of Sciences, Kol'tsovo, 630559 Russia
[c] Center of New Chemical Technologies, Boreskov Institute of Catalysis, Siberian Branch, Russian Academy of Sciences, Omsk, 644040 Russia
*e-mail: vinokurovzs@catalysis.ru

Abstract—We prepare a series of MnO_x–CeO_2 catalysts with a molar ratio of Mn : Ce = 3 : 7 by coprecipitation and varying the calcination temperature from 300 to 800°C. The catalysts are characterized by powder X-ray diffraction, low-temperature nitrogen adsorption, and X-ray photoelectron spectroscopy, and the catalytic activity of all samples is tested in the CO oxidation reaction. A $(Mn,Ce)O_2$ solid solution with the fluorite structure forms in all catalysts. Based on the studies performed, a catalyst calcined at 600°C is selected for further studies of the effect of topochemical reduction on the catalytic activity in the CO oxidation reaction by X-ray diffraction in the operando mode. The experiment is carried out sequentially in a stepwise mode: stepwise heating/cooling in a reaction mixture of 1% CO + 2% O_2 in the mode 150−175−200−175−150°C (stages 1, 3, and 5); reduction of the sample in a mixture of 10% CO + He at 400°C (stage 2); reduction of the sample in a mixture of 10% H_2 + He at 400°C (stage 4). The reductive treatment leads to segregation of the initial $(Mn,Ce)O_2$ solid solution and the appearance of dispersed manganese oxides on the surface, while enrichment of the surface with manganese oxide increases its activity in the CO oxidation reaction.

Keywords: cerium oxide, manganese oxide, $(Mn,Ce)O_2$, operando X-ray powder diffraction, CO oxidation

DOI: 10.1134/S1027451023030345

INTRODUCTION

To date, the preparation of active supported catalysts remains urgent in the development of heterogeneous catalysis. They are mainly obtained by applying the active component via impregnation of an oxide or carbon matrix (carrier). However, a method for obtaining such systems through topochemical reduction (redox exsolution) has recently been proposed [1]. In this method, the catalytically active metal element is first dissolved in the oxide matrix and then separated from the solid solution as catalytically active nanoparticles. The driving force behind this process is usually heat treatment in a reducing environment [2]; the application of an electrochemical potential can enhance the effect [3]. Obtaining nanoparticles by annealing in air was also studied using the nickel-doped electrode material $Ce_{0.9}Gd_{0.1}O_2$ as an example [4], but such treatment requires high temperatures, which can adversely affect the particle size and distribution density on the surface of the support [5]. The resulting nanoparticles are more uniformly distributed over the support surface and have a narrower size distribution compared to the supported catalyst conventionally obtained by vapor deposition or impregnation. These parameters can be controlled within certain limits [6]. Neagu et al. [7] showed that nanoparticles obtained by topochemical reduction have a strong bonding with the oxide substrate, which prevents the deactivation of active sites caused by particle agglomeration. One of the interesting effects is the stability to aging of the catalyst obtained by this method. For example, Nishihata et al. [8], using a palladium catalyst for the complete oxidation of exhaust gases based on perovskite, $LaFe_{0.57}Co_{0.38}Pd_{0.05}O_3$, demonstrated that cycling of the catalyst under redox conditions leads to reversible drift of palladium cations from the perovskite lattice. Due to this effect, the growth of palladium particles over time is suppressed and the activity of the catalyst is maintained at the same level.

Using the $(Mn,Zr)O_2$ solid solution with the fluorite structure as an example, we previously showed that under the conditions of a reducing CO and H_2 environment, manganese cations are released from the

initial oxide as dispersed MnO_x particles [9, 10]. Introducing an additional oxidation stage into the catalyst activation process also increased the catalytic activity in oxidation [11]. Presumably, analogous phenomena should occur in a solid solution based on cerium oxide.

This work is devoted to the operando study of the topochemical reduction of CO oxidation catalysts based on $(Mn,Ce)O_2$ solid solutions with the fluorite structure using X-ray diffraction. The work considers the processes of segregation of solid solutions with the formation of manganese oxides on the surface of a support, occurring both during the reductive treatment of the catalyst in H_2 or CO and under oxidizing conditions, including conditions of the catalytic oxidation of CO in excess oxygen.

EXPERIMENTAL

Synthesis

The initial manganese−cerium catalysts were prepared by coprecipitation from a solution of $Ce(NO_3)_3$ and $Mn(NO_3)_2$ salts. Synthesis was carried out similarly to that described in [9]. The Mn : Ce molar ratio for the series was 3 : 7. The obtained catalysts are denoted as Mn0.3Ce0.7_*T*, where *T* is the calcination temperature.

Ex Situ and Operando X-Ray Phase Analysis

The X-ray diffraction patterns of the catalysts were obtained using a D8 Advance powder diffractometer (Bruker, Germany) at $\lambda = 1.5418$ Å in the 2θ range from 23° to 83° with a step of 0.05° and an exposure time in one position of 5 s. An XRK-900 high-temperature reactor chamber (Anton Paar, Austria) was used for operando research. The heating rate was constant, 12°C/min; the gas-mixture supply rate to the chamber was 300 mL/min for a reaction mixture of 1% CO + 2% O_2 + He and 100 mL/min for the mixtures of 10% CO + He and 10% H_2 + He. The ICDD PDF-2 database [12] was used for qualitative phase analysis. Quantitative phase analysis and refinement of the lattice parameters were performed by the Rietveld method using the MAUD program [13].

X-Ray Photoelectron Spectroscopy

The chemical composition of the surface of the samples was studied using a SPECS photoelectron spectrometer (SPECS Surface Nano Analysis, Germany). The binding energy (E_b) scale was calibrated using the internal standard method by the Ce3$d_{3/2}$-U‴ peak of cerium, which is part of the support ($E_b = 916.7$ eV).

Measurement of the Catalyst Surface

The specific surface area was calculated by the Brunauer−Emmett−Teller method using nitrogen-adsorption isotherms measured at liquid-nitrogen temperatures using an ASAP 2400 automatic adsorption meter (Micromeritics, United States).

Catalytic Tests

The activity of the samples in the CO oxidation reaction was determined using a flow setup with a glass reactor (170 mm in length and 10 mm in diameter). The composition of the initial gas mixture was 1% CO and 99% air; the flow rate was varied within 253–487 mL/min to vary the contact time (τ). The CO conversion for each sample was determined at three values of the contact time. The weight of the sample (fraction 0.4–0.8 mm) was 0.2–1.5 g. The reaction temperature was 150°C. The composition of the reaction mixture before and after the reactor was determined using an LKhM-8MD chromatograph (Russia) with a column packed with Ca-A zeolite (3 m) and a thermal-conductivity detector. The activity A_{CO} of the catalyst (cm^3 g^{-1} s^{-1}) was calculated by the equation

$$A_{CO} = v_{CO}$$
$$\times \left| (P_{CO}/P_{N_2})_A - (P_{CO}/P_{N_2})_B \right| / \left[m_{cat} (P_{CO}/P_{N_2})_A \right],$$

where P_{CO} and P_{N_2} are the areas of CO and nitrogen peaks before (*A*) and after (*B*) the reaction (the area P_{N_2} was used as the internal standard); m_{cat} is the catalyst weight; and v_{CO} is the volumetric flow rate of CO.

Temperature-Programmed Reduction

Reduction in hydrogen was carried out using a flow setup with a thermal-conductivity detector. The sample was loaded into a quartz reactor, and a reductive mixture of 10 vol % H_2 in Ar was passed through it at a rate of 40 mL/min. The heating rate from room temperature to 900°C was 10°C/min.

RESULTS AND DISCUSSION

The phase composition and structural parameters of the catalysts of the Mn0.3Ce0.7_*T* series with a change in the calcination temperature from 300 to 800°C are presented in Table 1. According to X-ray diffraction data, the Mn0.3Ce0.7_*T* catalysts obtained at 300−600°C were single phase and represented a $(Ce,Mn)O_2$ solid solution based on the CeO_2 phase (PDF no. 34-394, space group $Fm\overline{3}m$, $a = 5.41134$ Å), as evidenced by the noticeably smaller lattice parameters ($a = 5.360(1)$ Å for Mn0.3Ce0.7_300) due to the difference in the ionic radii of the Ce and Mn cations. Judging from the gradual approach of the lattice parameter of the solid solution to the parameter of the

Table 1. Structural, microstructural, and surface characteristics of the Mn0.3Ce0.7_T series of catalysts. (Ce,Mn)O$_2$ is a solid solution based on cubic CeO$_2$ (PDF no. 34-394, space group $Fm-3m$, a = 5.41134 Å). [Mn]/[Mn + Ce] are the atomic ratios of elements in the near-surface layer of samples, obtained by X-ray photoelectron spectroscopy

Sample	Phase composition, wt %	Solid-solution lattice parameter, Å	Solid-solution coherent-scattering region, nm	Catalyst specific surface area, m^2/g	[Mn]/[Mn + Ce]
Mn0.3Ce0.7_300	(Ce,Mn)O$_2$	5.360(1)	6	80.6	0.29
Mn0.3Ce0.7_400	(Ce,Mn)O$_2$	5.3625(9)	7	72.5	0.29
Mn0.3Ce0.7_500	(Ce,Mn)O$_2$	5.3667(8)	7	57.0	0.27
Mn0.3Ce0.7_600	(Ce,Mn)O$_2$	5.3765(6)	7	40.8	0.28
Mn0.3Ce0.7_700	(Ce,Mn)O$_2$, 98.9 Mn$_3$O$_4$, 1.1	5.3962(3)	12	20.0	0.36
Mn0.3Ce0.7_800	(Ce,Mn)O$_2$, 90.6 Mn$_3$O$_4$, 2.1 Mn$_2$O$_3$, 7.3	5.4089(3)	29	9.2	0.37

pure CeO$_2$ phase, an increase in the calcination temperature causes the diffusion of manganese cations from the structure of the solid solution onto its surface. This process results in the formation of manganese oxide in a quantity sufficient for its detection by X-ray diffraction at a temperature of 800°C (~7 wt % of Mn$_2$O$_3$ for the Mn0.3Ce0.7_800 sample). An increase in the synthesis temperature also leads to particle sintering, which is characterized by an increase in the (Ce,Mn)O$_2$ coherent-scattering region from 6 to 29 nm and a decrease in the specific surface area of the catalysts from 80.6 to 9.2 m^2/g.

The data of X-ray photoelectron spectroscopy show similar dependences as those obtained by X-ray phase analysis (Table 1). For catalysts prepared at 300−600°C and representing a single-phase (Ce,Mn)O$_2$ solid solution, the [Mn]/[Mn + Ce] surface ratio is close to the stoichiometric value of 0.30. An increase in the calcination temperature leads to enrichment of the surface with manganese cations, the [Mn]/[Mn + Ce] ratio increases from 0.29 to 0.37, which is associated with the formation of manganese-oxide phases.

To assess the catalytic activity, we tested the samples in the CO oxidation reaction at a temperature of 150°C (Fig. 1). In the calcination temperature range of 300−500°C, we found a slight increase in activity from 5.1 × 10^{-2} to 5.8 × 10^{-2} cm^3 (CO) g^{-1} s^{-1}, followed by a sharp decrease to 0.3 × 10^{-2} cm^3 (CO) g^{-1} s^{-1} with a further increase in the calcination temperature to 800°C. As for the specific activity (normalized to the specific surface area of the sample), we observed a sharper increase in activity with an annealing temperature increasing from 300 to 500°C. This effect shows the relationship between the catalytic activity and the release of manganese to the surface of the solid

solution during annealing, which is essential for understanding the processes occurring at the atomic level. The Mn0.3Ce0.7_500 catalyst demonstrates the highest activity normalized to the surface. The specific activity of the Mn0.3Ce0.7_600 and Mn0.3Ce0.7_400 samples is at the same level, despite an almost twofold decrease in the specific surface. The latter may indicate the formation of new active centers, probably associated with MnO$_x$ on the surface of the solid solution, which is also evidenced by an increase in the amount of manganese, as follows from the results of X-ray photoelectron spectroscopy (Table 1). According to the published data , introducing manganese atoms into the CeO$_2$ lattice leads to the formation of oxygen vacancies, which form an active center capable of capturing and activating molecular oxygen [14]. Thus, the (Ce,Mn)O$_2$ solid solution has a higher activity in the CO oxidation reaction in comparison with CeO$_2$. MnO$_x$, in turn, has its own activity in oxidative reactions [15]. By analogy with our work on (Mn,Zr)O$_2$ [11], we decided to test the possibility of increasing the number of such active centers due to the release of manganese cations from the bulk of the solid solution by means of topochemical reduction, using the operando X-ray diffraction method.

To test this approach, we used the Mn0.3Ce0.7_600 catalyst. This selection was due to the maximum annealing temperature at which the sample is single phase according to X-ray diffraction data.

The curve of the temperature-programmed reduction of Mn0.3Ce0.7_600 in hydrogen (Fig. 2) contains three distinct hydrogen absorption peaks at temperatures of 259, 354, and 809°C. CeO$_2$ is characterized by two absorption peaks [16−18]. One peak at 300−500°C is associated with the reduction of surface oxy-
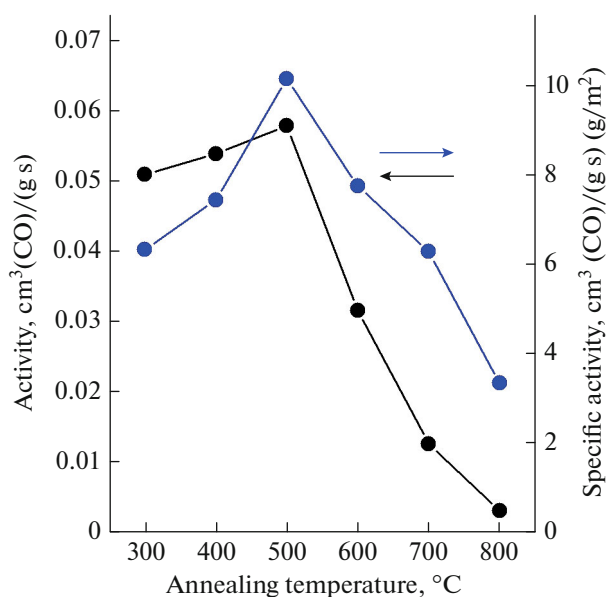
Fig. 1. Catalytic activity and specific activity (normalized to the specific surface area of the sample) calculated at 150°C for catalysts of the Mn0.3Ce0.7_T series depending on the catalyst preparation temperature.
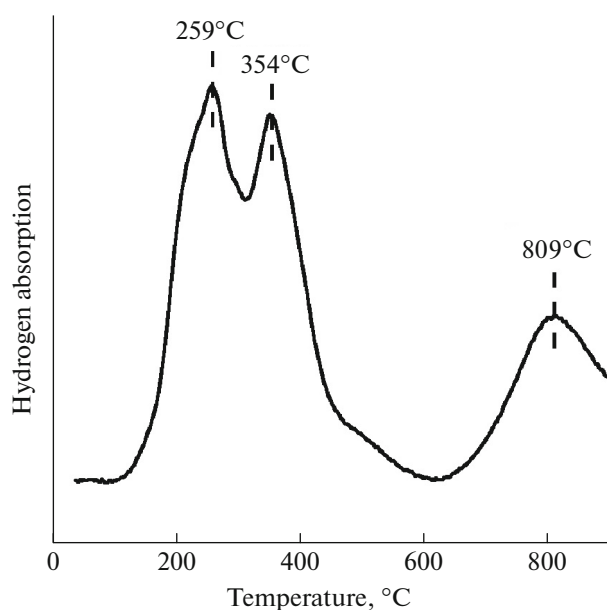

Fig. 2. Temperature-programmed reduction in hydrogen for the initial Mn0.3Ce0.7_600 catalyst.

gen and greatly depends on both the shape of the particles (tubes, cubes, rods [16]) and the amount and type of dopant in the complex oxide based on cerium oxide. For example, the doping of CeO_2 with iron shifts the first peak to lower temperatures [17], while the first peak of $Ti_xCe_{1-x}O_2$ is shifted to higher temperatures [18]. Another absorption peak is located in the temperature range of 650–900°C; it is associated with the reduction of oxygen in the bulk of fluorite. It is less susceptible to a form factor or a dopant effect. The reduction of Mn^{3+} and Mn^{4+} oxides occurs in the temperature range of 200–600°C and depends both on the structure of the oxide and the size of its particles [19] and on the bonding with the support. For example, an increase in the annealing temperature for TiO_2-supported manganese catalysts leads to the disappearance of the low-temperature peak corresponding to the reduction of MnO_2 to Mn_2O_3 due to interaction with the support [20]. For Mn0.3Ce0.7_600, the first two peaks of hydrogen absorption are most likely associated with the reduction of manganese cations either in the bulk of the solid solution or as segregated oxides $Mn^{4+} \rightarrow Mn^{3+}$ and $Mn^{3+} \rightarrow Mn^{2+}$, respectively. The reduction of the surface oxygen of the solid solution can also make a small contribution in the regions of the first two absorption peaks (~2/3 of the high-temperature absorption peak [16]). The high-temperature peak refers to the reduction of lattice oxygen in the pure CeO_2 phase. Based on these data, the reduction temperature of 400°C was selected to study

the processes of increasing catalytic activity due to topochemical activation.

A series of successive experiments were carried out as part of the study of the effect of various treatments on the structural characteristics and catalytic properties of the manganese–cerium catalyst Mn03Ce07_600. The stages were the following: study of the sample under stepwise heating/cooling in a reaction mixture of 1% CO + 2% O_2 in the mode 150–175–200–175–150°C keepeng for 2 h at each temperature simultaneously with the recording of reaction products (stages 1, 3, and 5), reduction of the sample in a mixture of 10% CO + He at 400°C for 2 h (stage 2), and reduction of the sample in a mixture of 10% H_2 + He at 400°C for 2 h (stage 4). The study of the sample without pretreatment in the CO oxidation reaction (stage 1) showed that heating after reaching a temperature above 175°C improves the CO conversion from 12 to 24% within 2 h; after reaching a temperature of 200°C, the conversion is 45% and stabilizes at 53% in 30 min (Fig. 3). Upon cooling after reaching each temperature, the conversion did not change; however, its values at each temperature exceeded those upon initial heating by ~5%. Segregation of the solid solution after the reaction was not observed (Fig. 4 and Table 2). However, a slight decrease in the lattice parameter from 5.3788(6) to 5.3762(6) Å was found, which may indicate an increase in the oxidation state of manganese. The reduction of the sample at 400°C in a 10% CO + He mixture (stage 2) led to the release of manganese from the solid solution and the forma-
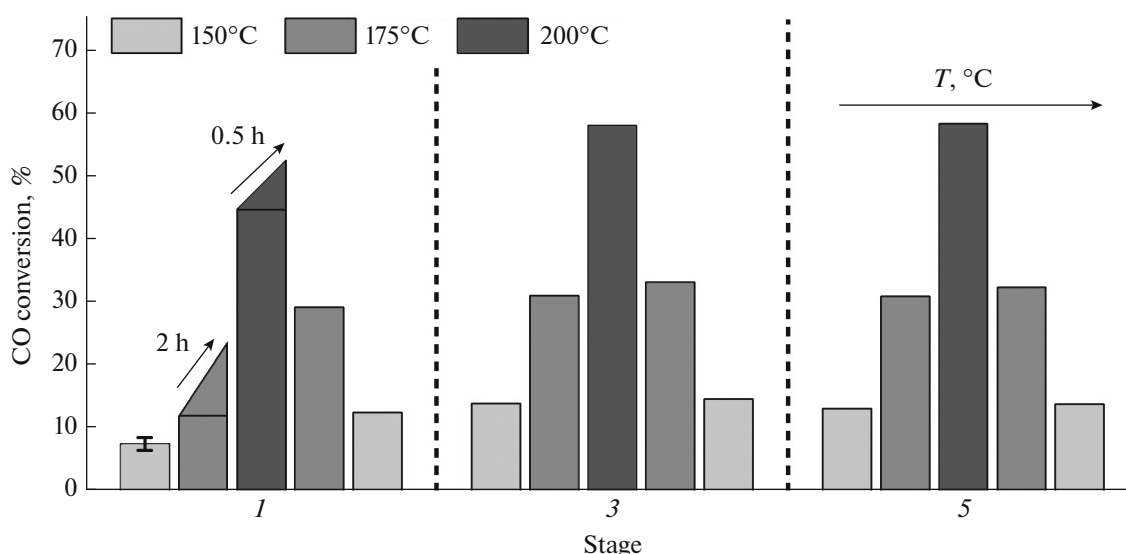
Fig. 3. CO conversion for the Mn0.3Ce0.7_600 sample at temperatures of 150, 175, and 200°C for (*1*) the initial sample and that after reduction in (*3*) CO and (*5*) H_2.

tion of the MnO phase (PDF no. 65-638, space group $Fm-3m$, a = 4.538 Å). Simultaneously with the appearance of the manganese(II) oxide phase, we observed a jump in the lattice parameter of the fluorite phase by over 0.2% and a decrease in the microstress value by 1.5 times. A repeated study of the system during CO oxidation (stage 3) showed the gradual disappearance of reflections corresponding to the MnO phase with increasing temperature. The most probable reason is the oxidation of MnO under the conditions of a catalytic reaction (1% CO + 2% O_2) into other phases of manganese oxides in a more dispersed state,

for example, Mn_2O_3 or Mn_3O_4, since the lattice parameter of the $(Mn,Ce)O_2$ phase, remaining the same, prevents the reverse incorporation of manganese. The activity of the sample increased slightly after reduction. The greatest difference was found at a reaction temperature of 200°C, at which the conversion changed from 53% (stage 1) to 58% (stage 3); this increase is most likely due to manganese oxides on the surface of the solid solution. Reduction in a 10% H_2 + He mixture showed similar results to those obtained in a 10% CO + He mixture. According to the X-ray diffraction data, the lattice parameter of the $(Mn,Ce)O_2$

Table 2. Results of X-ray phase analysis of the Mn03Ce07_600 sample obtained after various treatments at room temperature

| Treatment	Phase composition, wt %	Solid-solution lattice parameter, Å	Solid-solution coherent-scattering region, nm	Microstrain, %
Initial	$(Ce,Mn)O_2$	5.3788(6)	7	0.92(2)
After reaction, 1% CO + 2% O_2 200°C	$(Ce,Mn)O_2$	5.3762(6)	7	0.90(2)
After reduction, 10% CO 200°C	$(Ce,Mn)O_2$, 97.3 MnO, 2.7	5.3896(4)	8	0.67(1)
After reaction, 1% CO + 2% O_2 200°C	$(Ce,Mn)O_2$	5.3864(4)	8	0.71(1)
After reduction, 10% H_2 200°C	$(Ce,Mn)O_2$, 96.8 MnO, 3.2	5.3911(4)	8	0.65(1)
After reaction, 1% CO + 2% O_2 200°C	$(Ce,Mn)O_2$	5.3855(4)	8	0.71(1)
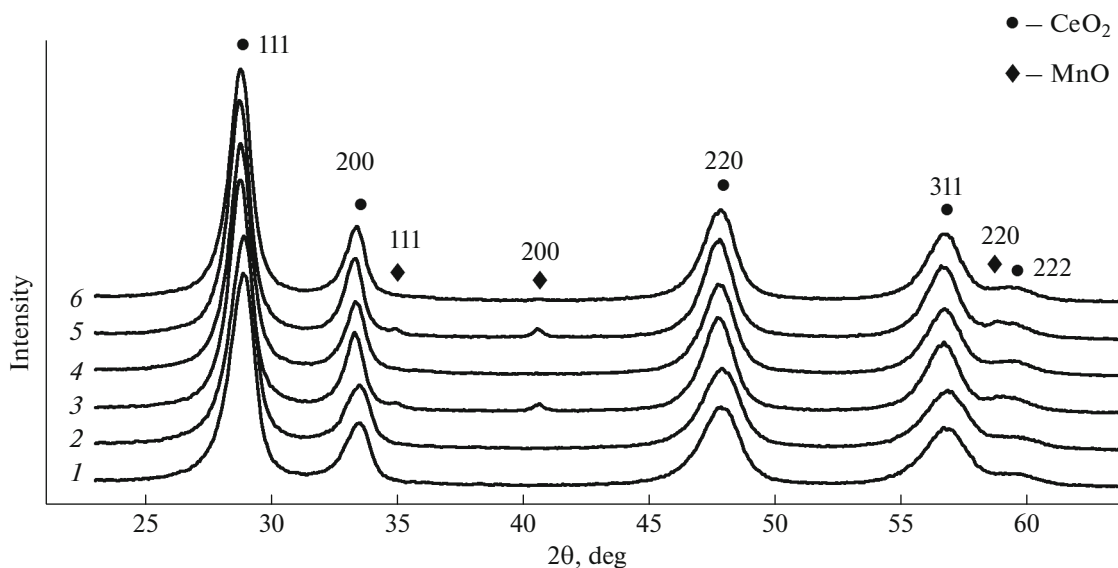
Fig. 4. X-ray diffraction patterns of the Mn0.3Ce0.7_600 sample obtained (*1*) in the initial state and after treatment in the reaction mixture at stages (*2*) 1, (*4*) 3, and (*6*) 5; (*3*) after reduction in a CO mixture at stage 2; (*5*) after reduction in a H_2 mixture at stage 4.

phase changed from 5.3896(4) Å at stage 3 to 5.3911(4) Å and a larger amount of MnO was formed (Table 2); apparently, hydrogen ensured the more manganese to drift from the solid solution.

Summing up, we synthesized a manganese–cerium solid solution with a fluorite structure and demonstrated that reduction treatment leads to the appearance of dispersed manganese oxides on the surface of the initial phase. In turn, this increases the activity of the system under study in the CO oxidation reaction. Nevertheless, no significant increase in the catalytic activity of Mn03Ce07_600 was observed after topochemical reduction. We believe that the main reason is that the diffusion of manganese from the bulk of the solid solution both creates new catalytically active sites associated with manganese-oxide nanoparticles and decreases their number in the solid solution.

CONFLICT OF INTEREST

The authors declare that they have no conflicts of interest.

REFERENCES

1. K. Kousi, C. Tang, I. S. Metcalfe, et al., Small **17**, 2006479 (2021).
   http://www.doi.org/10.1002/smll.202006479.2

2. D. Neagu, G. Tsekouras, D. N. Miller, et al., Nat. Chem. **5**, 916 (2013).
   http://www.doi.org/10.1038/nchem.1773

3. M. Chanthanumataporn, J. Hui, X. Yue, et al., Electrochim. Acta **306**, 159 (2019).
   http://www.doi.org/10.1016/j.electacta.2019.03.126

4. J. Tan, D. Lee, J. Ahn, et al., J. Mater. Chem. A **6**, 18133 (2018).
   http://www.doi.org/10.1039/C8TA05978K

5. S. -K. Otto, K. Kousi, D. Neagu, et al., ACS Appl. Energy Mater. **2**, 7288 (2019).
   http://www.doi.org/10.1021/acsaem.9b01267

6. J. Myung, D. Neagu, D. N. Miller, et al., Nature **537**, 528 (2016).
   http://www.doi.org/10.1038/nature19090

7. D. Neagu, T.-S. Oh, D. N. Miller, et al., Nat. Commun. **6**, 8120 (2015).
   http://www.doi.org/10.1038/ncomms9120

8. Y. Nishihata, J. Mizuki, T. Akao, et al., Nature **418**, 164 (2002).
   http://www.doi.org/10.1038/nature00893

9. O. A. Bulavchenko, Z. S. Vinokurov, T. N. Afonasenko, et al., Dalton Trans. **44**, 15499 (2015).
   http://www.doi.org/10.1039/C5DT01440A

10. O. A. Bulavchenko, Z. S. Vinokurov, T. N. Afonasenko, et al., Mater. Lett. **258**, 126768 (2020).
    http://www.doi.org/10.1016/j.matlet.2019.126768

11. O. A. Bulavchenko, Z. S. Vinokurov, T. N. Afonasenko, et al., Mater. Lett. **315**, 131961 (2022).
    http://www.doi.org/10.1016/j.matlet.2022.131961

12. S. Gates-Rector and T. Blanton, Powder Diffr. **34**, 352 (2019).
http://www.doi.org/10.1017/S0885715619000812

13. L. Lutterotti, Nucl. Instrum. Methods Phys. Res., Sect. B **268**, 334 (2010).
http://www.doi.org/10.1016/j.nimb.2009.09.053

14. G. Qi and R. T. Yang, J. Phys. Chem. B **108**, 15738 (2004).
http://www.doi.org/10.1021/jp048431h

15. K. Frey, V. Iablokov, G. Safran, J. Osan, et al., J. Catal. **287**, 30 (2012).
http://www.doi.org/10.1016/j.jcat.2011.11.014

16. G. Feng, W. Han, Z. Wang, et al., Catalysts **8**, 535 (2018).
http://www.doi.org/10.3390/catal8110535

17. L. Zhang, G. Spezzati, V. Muravev, et al., ACS Catal. **11**, 5614 (2021).
http://www.doi.org/10.1021/acscatal.1c00564

18. S. Watanabe, X. Ma, and C. Song, J. Phys. Chem. C **113**, 14249 (2009).
http://www.doi.org/10.1021/jp8110309

19. E. R. Stobbe, B. A. de Boer, and J. W. Geus, Catal. Today **47**, 161 (1999).
http://www.doi.org/10.1016/S0920-5861(98)00296-X

20. S. M. Lee, K. H. Park, S. S. Kim, et al., J. Air Waste Manage. Assoc. **62**, 1085 (2012).
http://www.doi.org/10.1080/10962247.2012.696532

Translated by O. Zhukova